

Performance of Coriolis Meters in Transient Gas Flows

Jodie G. Pope and John D. Wright

Sensor Science Division
National Institute of Standards and Technology
100 Bureau Drive, Gaithersburg, MD 20899-8361
Jodie.pope@nist.gov; john.wright@nist.gov

This manuscript is published in Flow Measurement & Instrumentation, Vol. 37, 2014; 42-53.

Abstract

For steady flows, Coriolis flow meters accurately measure mass flow. To study the performance of Coriolis meters under transient flows, we measured the instantaneous and totalized flow determined by two Coriolis meters. The tests used a Transient Flow Facility (TFF) developed to generate transient flow, pressure, and temperature conditions similar to those that occur when a hydrogen powered vehicle is refueled. During simulated cascade fills, the TFF discharged 3 kg of helium in 3 minutes at flows between 10 g/s and 45 g/s through the Coriolis meters and the TFF's standard. The TFF's expanded uncertainty (95 % confidence level) for totalized mass during this cascade fill was 0.45 %. For the same simulated cascade fill, both Coriolis meters measured the instantaneous flow within the uncertainty of the TFF and measured totalized flow within the International Organization of Legal Metrology Recommendation 139 maximum permissible errors for meters in gaseous fuel dispensers (1.0 %).

Keywords: Coriolis meter, gaseous fuel, hydrogen meter, time response, transient flow

1. Introduction

Flow meters are sometimes used to measure unsteady flows, under conditions where the temperature and pressure also vary. For example, dispensing stations for hydrogen-fueled vehicles comprise a set of pressure vessels (a cascade tube bank) filled to different pressures. As a vehicle is refueled, valves are sequentially opened to connect the vehicle's fuel tank to the cascade tubes in order of increasing pressure. As each tube is opened, surges of flow and pressure occur at the flow meter that totalizes the flow for customer billing. Rapid, large changes in temperature also occur due to flow work and the subsequent adiabatic cooling and heat transfer to the surroundings. Consumers and inspectors expect $< 1\%$ accuracy from meters used in gaseous fuel dispensers [1], but errors greater than 10% have been reported. At natural gas refueling stations, turbine meters subjected to pulsatile flow over-reported totalized flow by as much as 15% [2].

The National Institute of Standards and Technology (NIST) has constructed a Transient Flow Facility (TFF) to test gas flow meters under rapidly changing pressure, temperature, and flow conditions (Fig. 1). The TFF has four, 40 L high pressure tanks (HPTs) that serve as a source of nitrogen or helium¹ at an initial pressure of 42 MPa. These high pressure tanks can be sequentially discharged to simulate cascade filling of a vehicle. The gas is discharged in 3 to 5 minutes (depending on whether helium or nitrogen is used) into eight, 250 L low pressure tanks (LPTs) that are then the gas source for a 3-stage diaphragm compressor that periodically refills the HPTs back to 42 MPa. An extra set of 18 HPTs can also be pressurized so that flow can be maintained for > 1 min at nearly steady-state conditions. In this mode of operation, gas must be discharged to the atmosphere because the LPTs have insufficient capacity. The TFF can operate with any inert gas, although changing the gas requires approximately one week because successive evacuations and purges are required to assure gas purity.

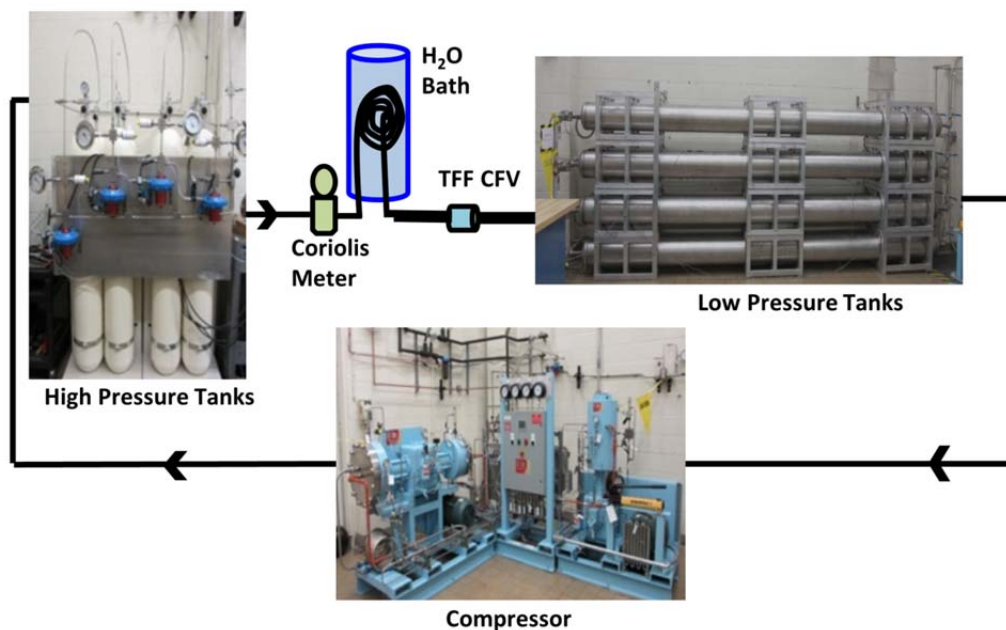


Figure 1: The Transient Flow Facility (TFF).

¹At the present time, only non-explosive and non-toxic gases can be safely used in the Transient Flow Facility.

The flow reference for the TFF is a 1 mm throat diameter, critical flow venturi (TFF CFV) with rapidly responding pressure and temperature sensors (< 20 ms) [3]. The TFF CFV has a flow calibration traceable to the NIST 677 L *PVTt* standard [4]. During transient flows, the gas density changes in the volume connecting the test section and the TFF CFV; therefore, the instantaneous flow through the meter under test (in this case a Coriolis meter) differs from the flow through the CFV. The flow due to this “storage effect” is larger than the CFV flow during the most extreme flow transients. The uncertainty of the instantaneous flow measurements is $< 24\%$ ($k = 2$)², and it is primarily driven by two apparatus-specific effects: 1) the response time of the pressure and temperature instrumentation associated with the TFF CFV and 2) the variation of the pressure and temperature measurements made in the connecting volume. Totalized mass flows during a simulated cascade fill have uncertainty $< 0.45\%$ ($k = 2$). Totalized uncertainties are much smaller than the instantaneous uncertainty due to the averaging of sensor variance and because the most extreme transients occur over only a small fraction of the total discharge time.

NIST used the TFF to test the performance of two Coriolis meters (Coriolis meter A and Coriolis meter B) under steady state flow conditions and during a simulated cascade fill. As presented later in this paper, both meters are capable of metering mass within the TFF uncertainty for both the instantaneous and the totalized flow measurements.

The gasses used in the TFF for the Coriolis meter tests were nitrogen and helium. When the TFF uses nitrogen, flows ranging from approximately 20 g/s to 120 g/s are achieved in the test section during the sequential discharge of the four HPTs, which correspond to Reynolds (*Re*) numbers of 6.7×10^5 to 4.0×10^6 . The total mass of nitrogen discharged by the four HPTs is approximately 11 kg in 5 minutes. The TFF uses helium to better simulate hydrogen gas refueling, and it allows for flows in the test section from approximately 10 g/s to 45 g/s, which correspond to *Re* numbers of 4.9×10^5 to 2.2×10^6 . The total mass of helium discharged by the four HPTs is approximately 3 kg in 3 minutes.

2. Calibration of the TFF reference CFV

The TFF operates at pressures up to 42 MPa; however, pressure losses in the plumbing reduce the maximum pressure to 39 MPa at the Coriolis meter and to 32 MPa at the TFF CFV. Before the Coriolis meters were tested, the TFF CFV was calibrated up to 29 MPa, the maximum steady pressure that could be maintained. As previously described in reference [5], the TFF CFV was calibrated in nitrogen up to 10 MPa using the NIST 677 L *PVTt* flow standard. Additional calibrations up to 29 MPa were performed by installing in series with the TFF CFV individual larger, calibrated “working standard” CFVs that had been calibrated with the 677 L *PVTt* flow standard. As shown in Fig. 2, all 22 HPTs were filled with nitrogen and a pressure regulator and heat exchangers were used to achieve approximately steady state conditions at the two CFVs. The gas was vented to the atmosphere to prevent over pressurization of the LPTs and to ensure that critical flow conditions were maintained across the CFVs. The series arrangement of CFVs allowed us to calibrate the TFF CFV at pressures up to 29 MPa while the working standard CFVs were subjected to pressures between 200 kPa and 700 kPa (as calibrated in the *PVTt* standard). Three working standard CFVs with throat diameters of 1.60 mm, 3.18 mm, and 6.35 mm were necessary to calibrate the TFF CFV with an uncertainty of 0.12% ($k = 2$).

² Uncertainties will be labeled $k = 1$ or $k = 2$ depending on their confidence levels of approximately 68% or 95.5%.

The TFF CFV is instrumented with both “fast” and “slow” pressure and temperature sensors. The slow sensors, with time constants on the order of 1 s, were installed in parallel with fast sensors: the slow sensors were used under steady state conditions to re zero the fast sensors before each test. The fast pressure sensor has a manufacturer specified time constant of 5 ms. The fast temperature sensors were two, redundant, exposed junction Type K thermocouples with wire diameter of 0.05 mm welded onto 0.25 mm supports within a 3 mm insertion tube. The measured time constant of the thermocouples was < 20 ms at the gas velocities typical of the TFF [3]. The TFF software and hardware acquire measurements with a period of 10 ms.

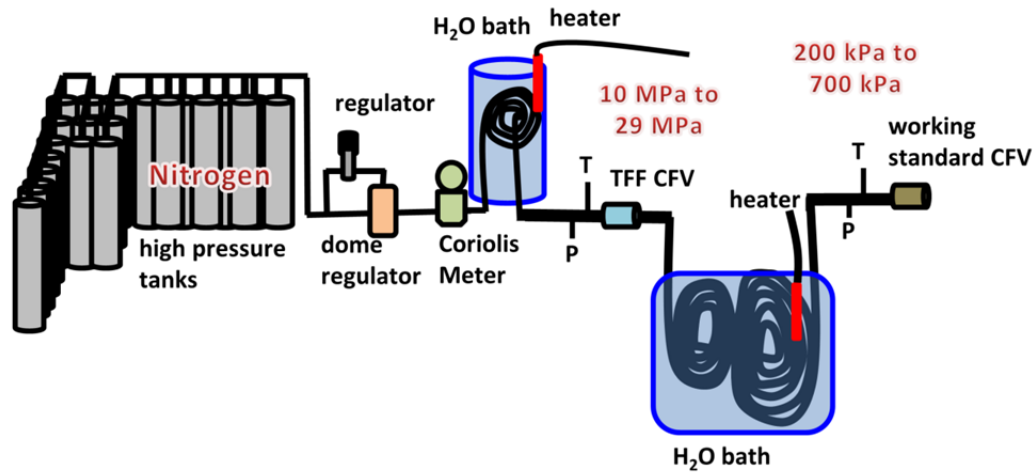


Figure 2: Setup for the steady state calibration of the TFF CFV.

Fig. 3 shows samples of the stagnation pressures and temperatures at the TFF CFV and at the 3.18 mm working standard CFV for three flows during the steady state calibrations. Only measurements where storage effects introduced no more than 0.03 % flow instability between the two CFVs were used. The windows in Fig. 3 indicate the portions of data averaged for the TFF CFV calibration of three flows at 13.3 g/s, 8.2 g/s, and 3.6 g/s.

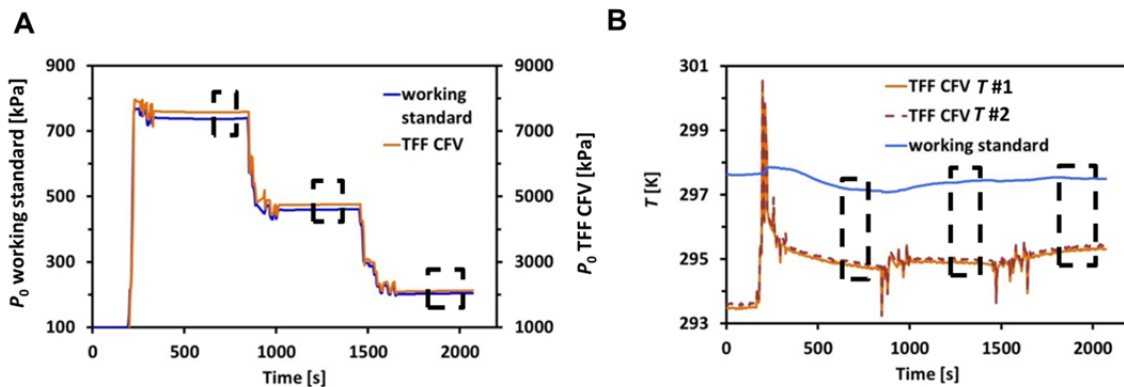


Figure 3: Stagnation pressures (A) and temperatures (B) at the TFF CFV and at the 3.18 mm

working standard CFV during the collection of three calibration points.

The reference mass flow through the working standard CFV is:

$$\dot{m}_{ws} = \frac{C_d P_0 A C^* \sqrt{M}}{\sqrt{RT_0}} = C_d \dot{m}_{th}, \quad (1)$$

where C_d is the working standard CFV discharge coefficient, \dot{m}_{th} is the theoretical mass flow, P_0 and T_0 are the stagnation pressure and temperature, A is the throat area, C^* is the real gas critical flow function [6,7], M is the molar mass, and R is the universal gas constant. At steady state and in the absence of leaks from the connecting volume, the mass flow through the working standard CFV is equal to that through the TFF CFV, and therefore C_d for the TFF CFV is:

$$C_{d, \text{TFF CFV}} = \frac{\dot{m}_{ws}}{\dot{m}_{th, \text{TFF CFV}}} = \frac{C_{d, ws} P_{0, ws} A_{ws} C_{ws}^* \sqrt{T_{0, \text{TFF CFV}}}}{P_{0, \text{TFF CFV}} A_{\text{TFF CFV}} C_{\text{TFF CFV}}^* \sqrt{T_{0, ws}}}. \quad (2)$$

Averages from steady state windows like those in Fig. 3 were processed via Eq. 2 to obtain C_d values for the TFF CFV and are plotted versus the inverse square root of the theoretical Reynolds number³ Re_{th} (points in Fig. 4). A rational polynomial was fitted to the calibration points (also shown in Fig. 4) and this curve fit was the basis for subsequent TFF CFV flow measurements. The presentation of CFV data as C_d vs. $1/\sqrt{Re_{th}}$ linearizes the discharge coefficient plot for the CFV laminar boundary layer regime [8]. The decline in C_d at low $1/\sqrt{Re_{th}}$ values (high Re_{th} values) is due to the boundary layer in the CFV undergoing the laminar to turbulent transition. As shown in prior research [9], operating in the transition regime does not degrade the quality of the calibration. The offset between C_d values from the three working standard CFVs and the NIST 677 *PVTt* standard at overlapping Re numbers in Fig. 4 are never > 0.02 %.

³ The theoretical Reynolds number Re_{th} is based on the theoretical mass flow (not the real mass flow), i.e. $Re_{th} = 4\dot{m}/(\pi d\mu)$ where d is the CFV throat diameter and μ is the dynamic viscosity. This expression has advantages over the real Re because it eliminates the need for iteration to obtain the discharge coefficient when the CFV is used to measure flow.

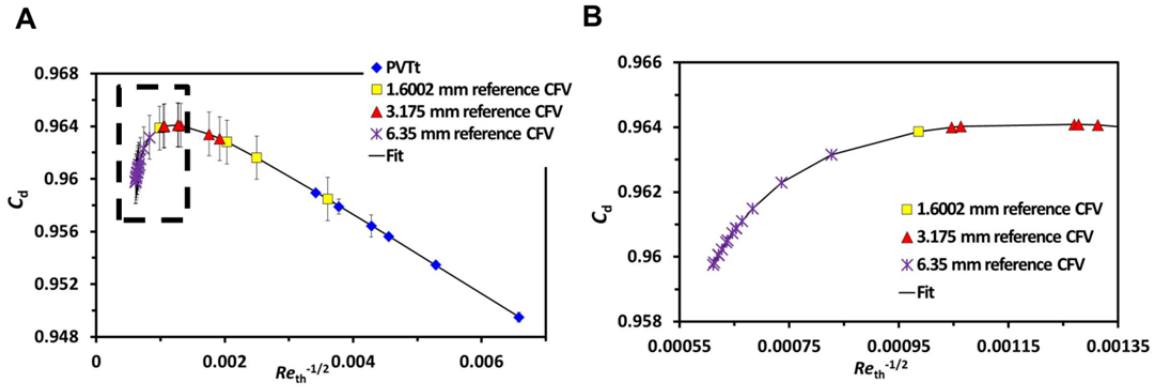


Figure 4. A) Discharge coefficient (C_d) data for the TFF CFV. The outlined area shows the part of the curve used in the TFF. Error bars represent the uncertainty of the discharge coefficient. B) Expanded view of the curve used in the TFF.

The calibration shown in Fig. 4 was performed using nitrogen, and additional uncertainty must be considered if the same calibration curve is assumed for a different gas species. For example, prior research shows a difference between nitrogen and helium CFV calibration curves of 0.5 % at $1/\sqrt{Re_{th}} = 0.01$, but the difference diminishes as $1/\sqrt{Re_{th}}$ decreases and the CFV boundary layer thins [8,10]. At the low $1/\sqrt{Re_{th}}$ values over which the TFF CFV is used, species effects are predicted to contribute < 0.02 % ($k = 1$) to the flow uncertainty.

3. Transient flow measurements with the TFF

When the TFF is used during transient flow conditions, storage effects, *i.e.* density changes in the volume connecting the meter under test and the TFF CFV, must be taken into account. The mass flow exiting the test section (\dot{m}_{TFF}) is equal to the mass flow through the CFV (\dot{m}_{CFV}) plus the flow due to density changing in the connecting volume (\dot{m}_c):

$$\dot{m}_{TFF} = \dot{m}_{CFV} + \dot{m}_c = \frac{C_d P_0 A C^* \sqrt{M}}{\sqrt{RT_0}} + V_c \frac{d\rho}{dt} \cong \frac{C_d P_0 A C^* \sqrt{M}}{\sqrt{RT_0}} + V_c \frac{\Delta\rho}{\Delta t}, \quad (3)$$

where V_c is the connecting volume, $\Delta\rho$ is the change in the density in V_c during the time Δt between the acquisition of two consecutive data points (10 ms in this case). Storage effects are most significant at the start of a simulated cascade fill when the first HPT is opened and the pressure in V_c rises from 0.5 MPa to over 32 MPa in less than 2 s. The pressurization causes the fast thermocouple readings to rise to 325 K in less than 1 s (See Figs. 5A and 5C.); thereafter, the temperature decreases to the temperature of the water in the heat exchanger. When a HPT is first opened, the connecting volume flow is as much as 7 times that through the TFF CFV. See Figs. 5B and 5D.

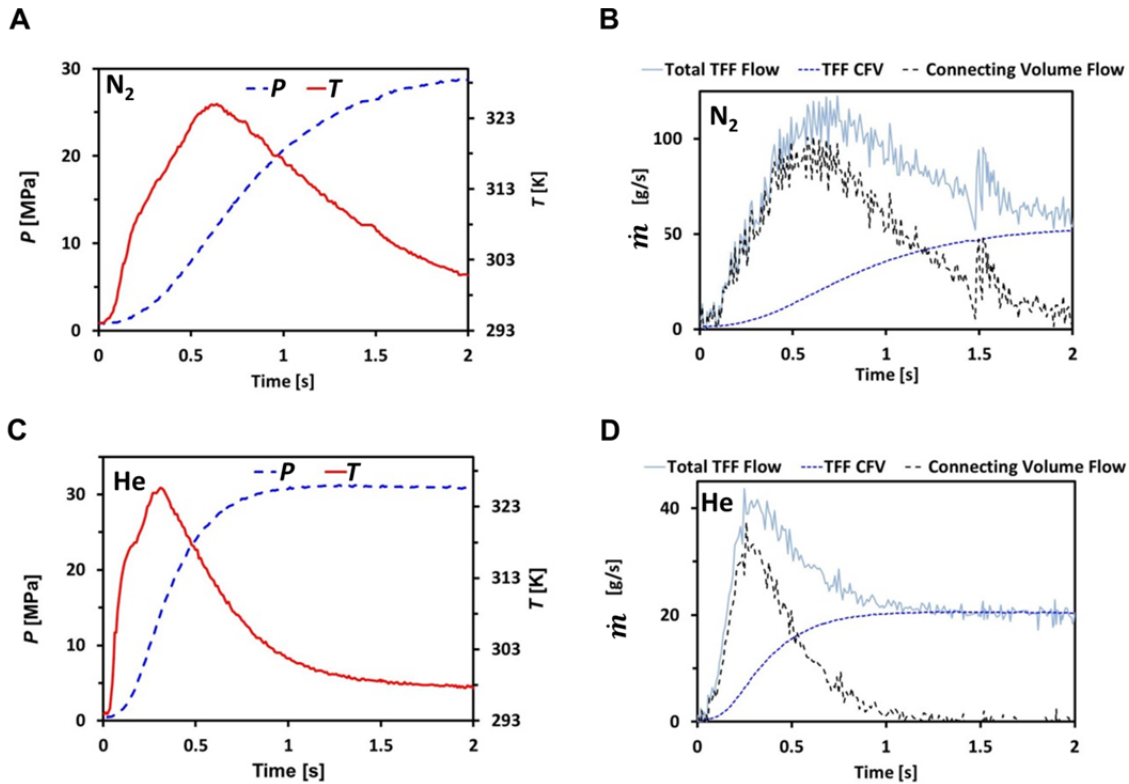


Figure 5. A) The stagnation pressure and temperature profile at the CFV during the initial discharge of a nitrogen HPT. B) TFF CFV flow and connecting volume flow during the initial nitrogen discharge. C) The stagnation pressure and temperature profile at the CFV during the discharge of one helium HPT. D) CFV flow and connecting volume flow for a helium discharge.

The pressure and temperature time dependences for nitrogen and helium differ: the maximum temperature and pressure for helium occur in approximately half the time for nitrogen and the resulting initial flow transient is shorter. This can be explained as follows. For a given pressure and temperature applied to a choked flow inlet, the volumetric flow of helium entering the connecting volume is 2.1 times larger than the volumetric flow of nitrogen because the speed of sound is higher in helium than in nitrogen. Therefore, the connecting volume fills to the maximum pressure more rapidly. If hydrogen were used in the TFF, the initial flow transient would be shorter still: the hydrogen volumetric flow would be 2.9 times the nitrogen volumetric flow, or equivalently, 1.4 times the volumetric flow of helium.

The connecting volume flow determined from the temperature and pressure readings and the equation of state is highly sensitive to noise. The fastest TFF CFV measurements (taken with a 10 ms period) show large fluctuations in mass flow (see Figs. 5B and 5D) that can be traced to the variance of the numerically calculated derivative of the density with respect to time. Alternatively, for data presentation with less noise, the density *versus* time data can be filtered by fitting it with a rational polynomial and using the time derivative of this curve fit to calculate the mass flow in the connecting volume.

The detailed uncertainty analysis in Section 6 gives the uncertainty of: 1) the instantaneous mass flow measurements made by the TFF and 2) the totalized mass metered for a simulated cascade fill. The expanded uncertainty in the mass flow at any instant is as high as 24 % at the initial discharge of a

HPT and it decreases to 14 % as the tank depletes ($k = 2$). The largest uncertainty components in instantaneous mass flow are $\Delta\rho$ in the connecting volume and the standard deviation of the flow measurements, σ_{noise} , a consequence of fluctuating temperature and pressure measurements.

The totalized mass flow uncertainty for a simulated cascade fill is 0.45 % ($k = 2$), significantly lower than the instantaneous flow uncertainty because the standard deviation of the instantaneous measurements can be neglected due to cancellation of noise during integration. The largest contributing components to the uncertainty in totalized mass metered are the C_d for the TFF CFV and $\Delta\rho$ in the connecting volume.

Obtaining accurate storage effect flows requires low uncertainty measurements of 1) the connecting volume and 2) the spatially averaged density in the connecting volume. The size of the connecting volume was measured by isolating it with closed valves and a cap and using the volume expansion method with a 0.5 L reference volume [11]. Ideally, the temperature and pressure values used to calculate the gas density would be spatial averages of the values in the connecting volume; however, in practice sensors are installed at limited yet strategic locations. To obtain a better approximation of the spatial average, the connecting volume was divided into sub volumes defined by the locations of pressure drops due to valves and elbows or the locations of temperature changes due to the heat exchanger. The sub volumes were temporarily instrumented with extra pressure and temperature sensors to determine the relationship between the desired volume weighted pressure and temperature and the pressure and temperature measured at the permanent sensor locations. The details of this can be found in Section 6.2.

4. Steady flow calibrations of the Coriolis meters

Figs. 6A and 6B show the results of the steady state calibration of Coriolis meters A and B, respectively. Coriolis meter A was calibrated against the working standard CFVs and Coriolis meter B against the TFF CFV. The standard deviation (represented by the error bars in Fig. 6) of the calibration data for Coriolis meter A is greater than that for Coriolis meter B because the regulator that controls the outlet pressure to the test section was upgraded between their tests. We emphasize that the Coriolis meters were installed upstream from any heat exchanger and therefore were exposed to larger temperature changes than those shown in Fig. 3. The calibrations spanned steady nitrogen flows from 10 g/s to the TFF maximum of 55 g/s. During simulated cascade filling, nitrogen flows ranged from 20 g/s to 120 g/s and helium flows ranged from 10 g/s to 45 g/s.

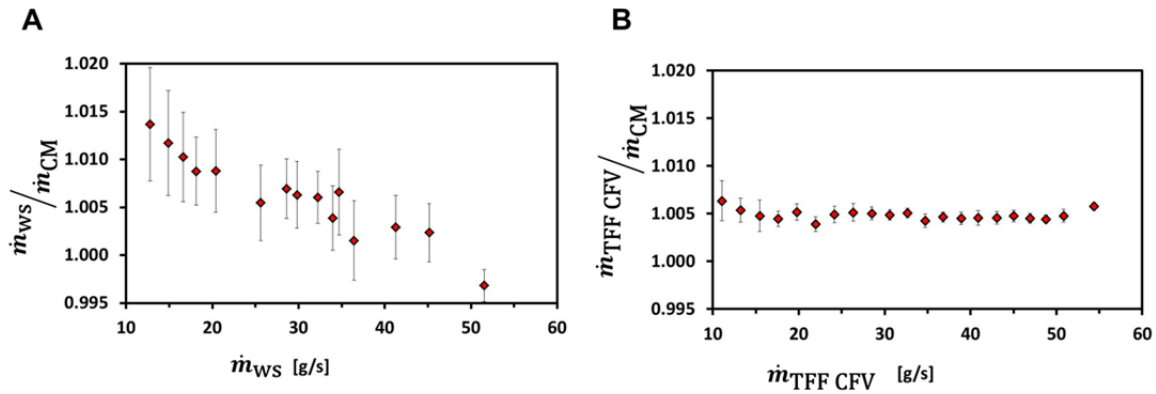


Figure 6. A) Steady state flow calibration results for Coriolis meter A. B) Steady state calibration results for Coriolis meter B. Error bars are standard deviations of the ratio of the mass flow indicated by the Coriolis meter to the reference mass flow.

5. Transient flow measurements with the Coriolis meters

Comparisons between the TFF CFV and the Coriolis meters were made during simulated cascade fills to test the Coriolis meters' ability to measure the total mass discharged from a gaseous refueling dispenser. Fig. 1 shows the setup for the transient measurements. Four of the HPTs were opened and closed sequentially, generating pressure and temperature transients similar to those shown in Fig. 7. The instantaneous flow measurements and the totalized flows during the simulated cascade fill (outlined region in Fig. 7) from the TFF and the Coriolis meters were compared. Data from the 4 to 20 mA outputs of the Coriolis meters were acquired at 100 Hz along with the other TFF measurements.

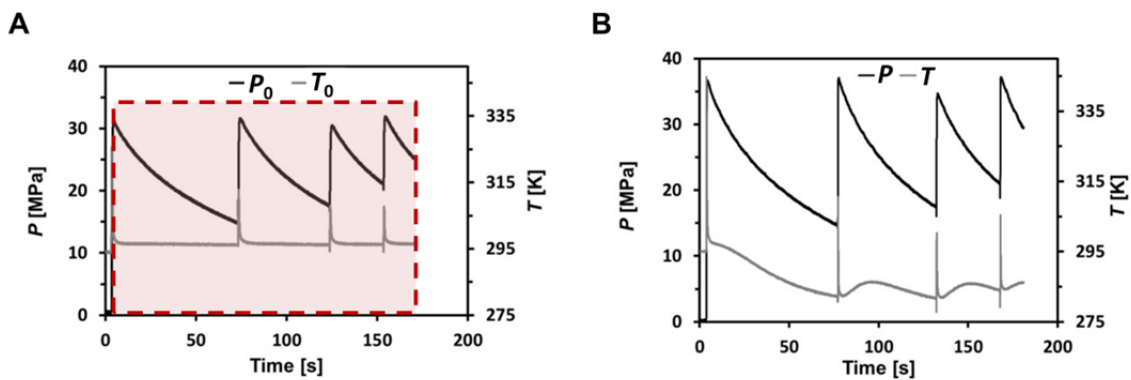


Figure 7. A) Stagnation pressure and temperature profile at the TFF CFV during the sequential discharging of the four HPTs filled with helium. The shaded, outlined region shows the part of the corresponding mass flow curve that is included for totalized mass metered determination. B) The P and T profile at the Coriolis meter.

5.1. Coriolis meter A

Coriolis meter A has three settings that influence the meter response: 1) low flow cut-off, 2) time constant⁴ (“damping”), and 3) lag time (“response latency”). For the initial cascade fill simulations conducted with nitrogen, the lag time was 0.075 s and the low flow cut-off was set to zero. Figs. 8A, 8B, and 8D show the results for time constant settings of 0.32 s, 0.16 s, and 0 s during the first two seconds following the discharge of one HPT. The variance in the TFF flow in Fig. 8A is introduced by the storage effects term and noise in the connecting volume pressure and temperature data. As expected, the amplitude of the Coriolis output decreases and the lag increases for larger time constant settings. The maximum flow registered by the Coriolis meter is at least 20 % lower than that reported by the TFF, even for the 0 s time constant setting. The influence of the nonzero lag setting is evident in the approximately 0.05 s delay between the rise in the TFF flow measurement and the Coriolis meter output. Fig. 8C shows that there is no significant difference in the variance of the Coriolis data for the three time constant settings.

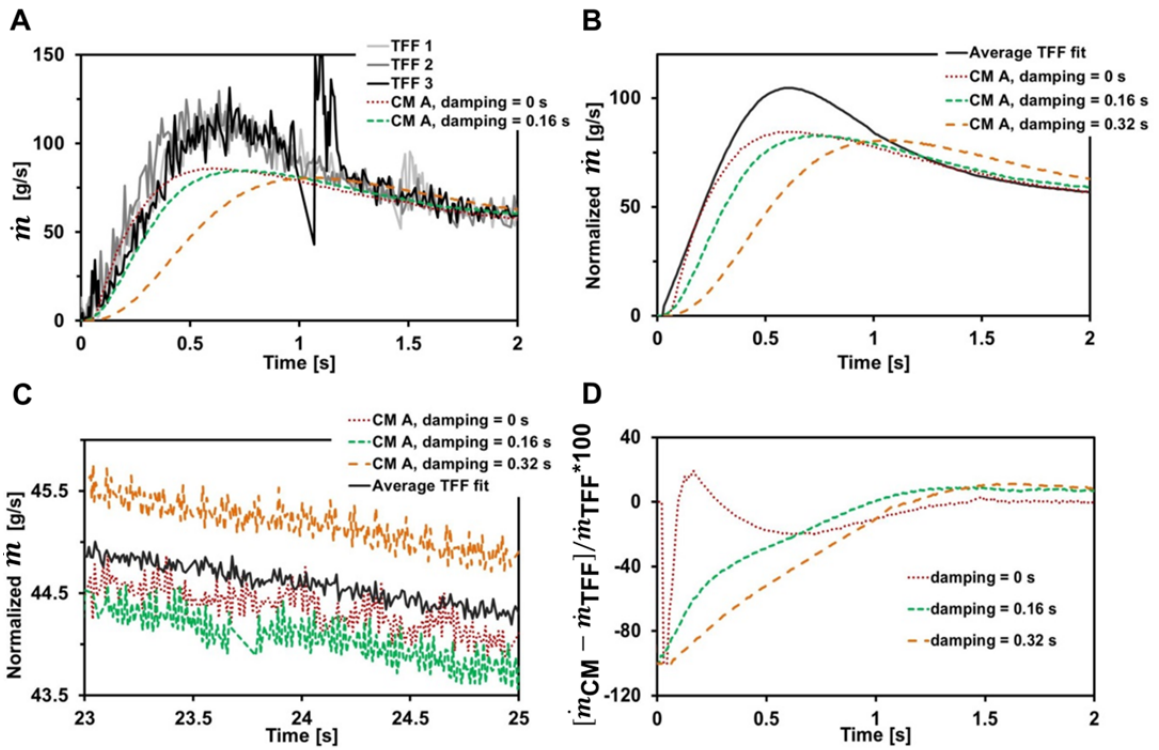


Figure 8. A) The response of Coriolis meter A (CM A) to the discharge of nitrogen from the HPT with various flow damping values applied. The TFF flow for all three cascade fills is shown. B) The curves from “A” but normalized to the TFF flow measurement. The TFF curve is a curve fit to the average of the three CFV response curves shown in A. C) A sample of data from later stages of the HPT depletion. The time constant does not affect Coriolis meter A variance. D) The percent difference in mass flow of Coriolis meter A compared to the TFF for the various time constants.

Coriolis meter A was assessed again with helium. The low flow cut-off and the time constant were left at zero. Figs. 9A and 9B compare the responses for two lag values: 0.075 s and the minimum

⁴ Time constant is the interval required for the meter output to reach 63.2 % of the final value when exposed to a step change in input.

value of 0.035 s. Note that the TFF flow measurements also have an estimated lag of 0.02 s resulting from the time constants of the pressure and temperature sensors used to calculate the reference flow.

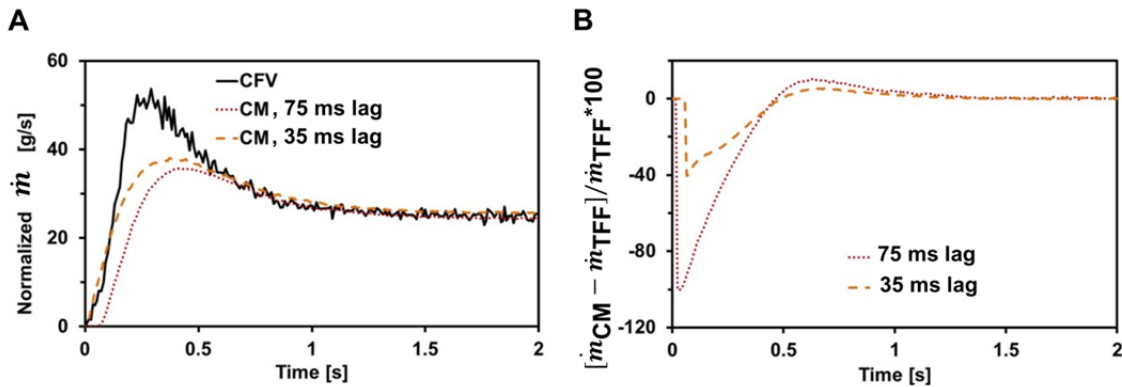


Figure 9. A) The response of Coriolis meter A to the discharge of helium from the HPT with lag values of 0.035 s and 0.075 s. The average response of the TFF from eight test runs is shown and the Coriolis meter responses have been normalized. B) The percent difference in mass flow of Coriolis meter A compared to the TFF mass flow for the different lag settings.

Totalized mass comparison for Coriolis meter A

Figs. 10A and 10B show the mass flow measured by the TFF and Coriolis meter A during a simulated cascade fill using nitrogen and helium, respectively. The area under these curves gives the totalized mass metered by the TFF and the Coriolis meter. Table 1 summarizes the tests of Coriolis meter A for various flow meter settings and gases. Three Coriolis meter calibration options were tested and are shown as separate columns in Table 1. 1) “As received calibration and field zeroing”: the as received calibration was used with a field zeroing with the Coriolis meter’s user interface. (For field zeroing, the zero feature was set after the test section was filled to approximately 10 MPa and valves upstream and downstream of the Coriolis meter were closed.) 2) “Additional zeroing”: the Coriolis meter indicated a negative flow under the no flow condition despite the field zeroing procedure. This negative zero flow reading remained stable from day to day (approximately $-0.113 \text{ g/s} \pm 0.025 \text{ g/s}$), and it was subtracted from the acquired flow data before integration. 3) “Additional zeroing and calibration”: the negative zero flow reading was removed as for option 2 and a gain correction (1.0029) was applied based on the TFF steady state flow calibration shown in Fig. 6A. The first option is available to all Coriolis meter users while the second and third options are available only to users who use a data acquisition system and perform their own meter calibration.

With the as received calibration and field zeroing (calibration option 1), totalized flows from Coriolis meter A and the TFF agreed within 1.05 % for all meter settings. By applying the additional zeroing (calibration option 2), the difference in totalized flows was < 0.49 %. Calibration option 3 cut the difference in half again to < 0.2 %. The good agreement is somewhat surprising considering that the Coriolis meter under reported flow by 20 % during the initial HPT discharge, but the initial transient following the discharge peaked at 0.3 s to 0.5 s while the entire flow test lasted 180 s to 300 s. For Coriolis meter A in this simulated cascade fill, the various time constant and lag settings examined

have negligible effect on the totalized flow accuracy. However, this may not hold true if the meter were exposed to transient flows with larger and/or more frequent flow fluctuations.

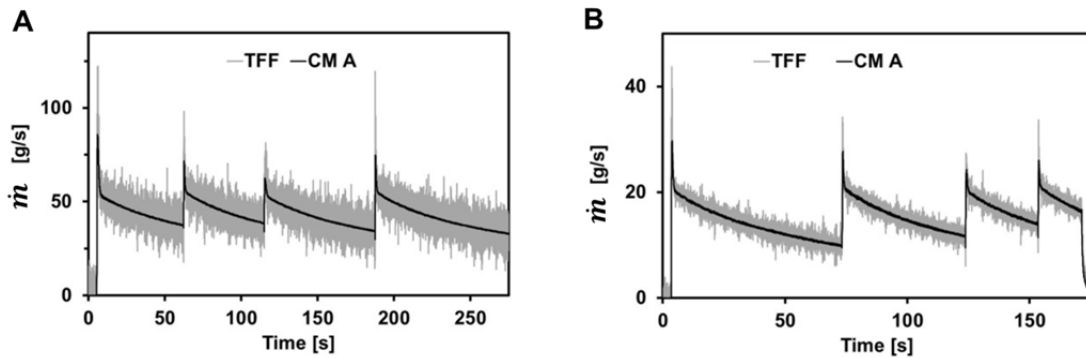


Figure 10. Mass flow profile during the discharge of the TFF's four HPTs. A) Nitrogen. B) Helium.

Table 1. Percent difference in totalized mass metered by Coriolis meter A and the TFF during simulated cascade refueling. The last column gives the standard deviation of the mean.

Gas	Time constant (s)	Lag (s)	Number of tests, n	1) As received calibration and field zeroing (%)	2) Additional zeroing (%)	3) Additional zeroing and calibration (%)	$\frac{s}{\sqrt{n}}$ (%)
N ₂	0.32	0.075	2	-0.81	-0.49	-0.2	0.04
N ₂	0.16	0.075	4	-0.61	-0.31	-0.2	0.02
N ₂	0	0.075	2	-0.81	-0.49	-0.2	0.03
He	0	0.075	2	-1.05	-0.49	-0.2	0.07
He	0	0.035	6	-0.94	-0.36	-0.06	0.09

5.2 Coriolis meter B

The instantaneous and totalized flows output by Coriolis meter B were compared to the TFF during simulated cascade fills using nitrogen and helium gas. Coriolis meter B has a user selectable time constant and a digital low pass filter (LPF) that can be set to an integer number of flow tube oscillation cycles (1 is the minimum value). The as received values for the time constant and LPF were 0.8 s and 64 cycles, respectively.

Fig. 11 shows the mass flow for Coriolis meter B and the TFF during the first 5.5 seconds following the discharge of nitrogen from the HPT at each time constant setting. The time constant settings were altered to examine the effects of flow damping on the response of Coriolis meter B to the

opening of one of the HPTs. The first measurements were made with the as received values of 0.8 s for the time constant, 1.0 % low flow cut-off limit and 64 for the LPF. The next measurements were made with the LPF set to its minimum value of 1, the low flow cut-off limit removed, and the time constant decreased, first to 0.10 s and then to the minimum value allowed, 0.05 s.

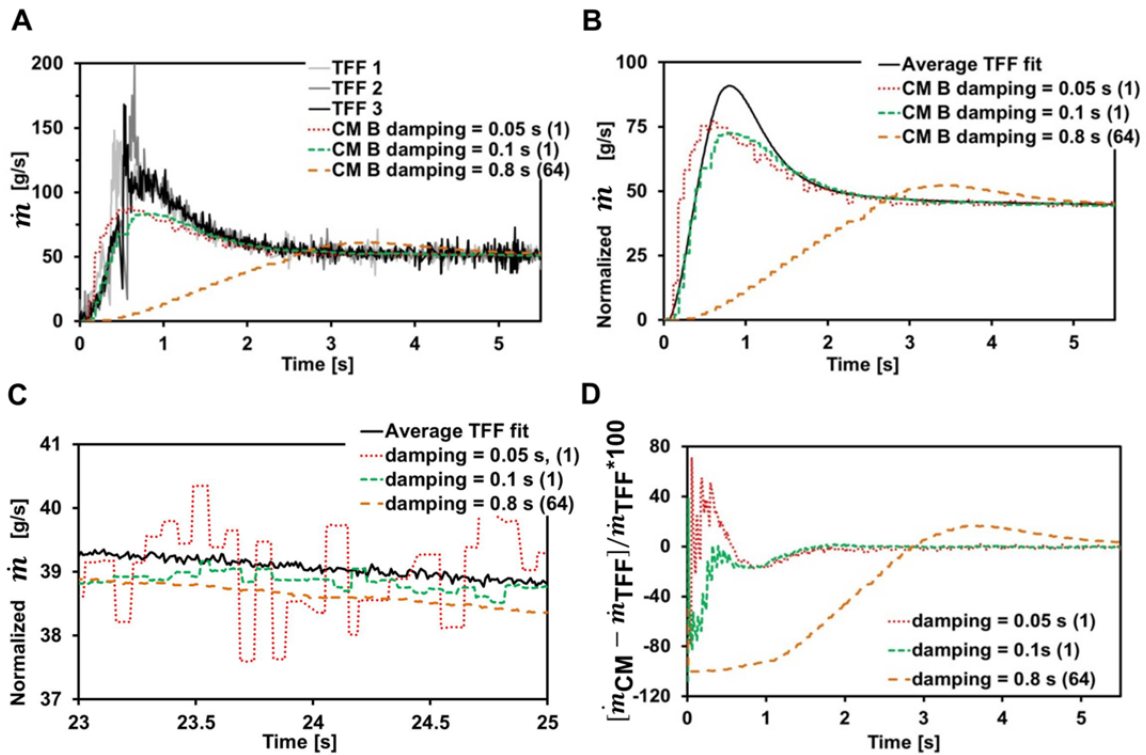


Figure 11. A) The response of Coriolis meter B (CM B) to the discharge of nitrogen from the HPT with various time constant values applied. The TFF flow for each simulated cascade fills is also shown. B) The curves from “A” but normalized to the TFF flow measurement. The TFF curve is a curve fit to the average of the three CFV response curves shown in “A”. C) A sample of data from later stages of the HPT discharge showing the time constant effect on meter output variance. D) The percent difference in mass flow indicated by Coriolis meter B compared to the TFF for the various time constants.

Coriolis meter B was assessed again with helium. The low flow cut-off was removed and the time constant was left at the minimum value of 0.05 s. Figs. 12A and 12B show the response of Coriolis meter B to the discharge of helium from one HPT compared to the TFF.

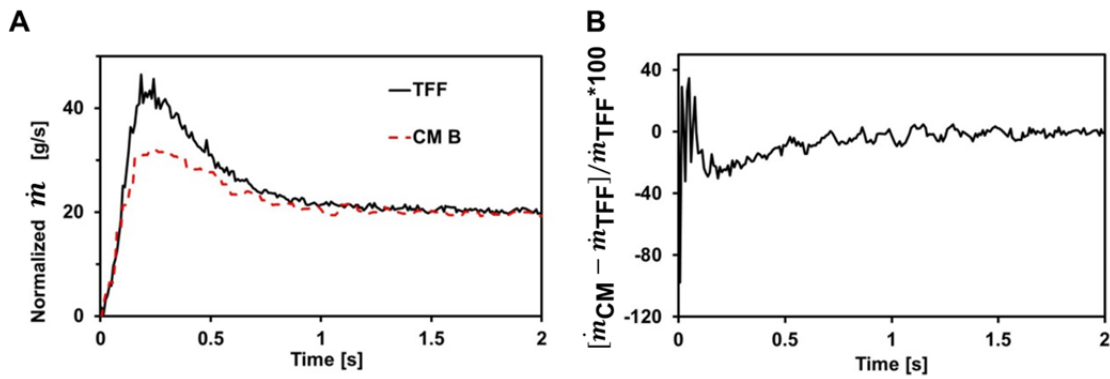


Figure 12. A) The response of Coriolis meter B (CM B) to the discharge of helium from the HPT. The average response of the TFF from five measurements is shown. The Coriolis meter response has been normalized to the TFF curve. B) The percent difference in mass flow between Coriolis meter B and the TFF.

Totalized mass comparison for Coriolis meter B

The differences between the TFF and Coriolis meter B totalized flows were calculated using the same three calibration options explained for Coriolis meter A. The difference between Coriolis meter B and the TFF for a simulated cascade fill was $< 0.84\%$ for all of the tested meter settings (see Table 2). When the time constant and LPF settings were reduced, the differences were within 0.23% . For the third calibration option, two gain values were used to apply the calibration corrections of Fig. 6B: at the lower flows that apply to helium the gain correction was 0.9983 while at higher nitrogen mass flows, the correction was 1.0004.

Table 2. Percent difference in totalized mass metered by Coriolis meter B and the TFF during simulated cascade refueling.

Gas	Time constant (s)	Low pass filter (cycles)	Number of tests, n	1) As received calibration and field zeroing (%)	2) Additional zeroing (%)	3) Additional zeroing and calibration (%)	$\frac{s}{\sqrt{n}}$ (%)
N ₂	0.8	64	2	-0.84	-0.58	-0.58	0.14
N ₂	0.1	1	3	-0.23	-0.05	-0.01	0.04
N ₂	0.05	1	3	-0.20	-0.08	-0.04	0.03
He	0.05	1	5	-0.24	0.29	0.12	0.03

6. Uncertainty analysis

The uncertainty of the instantaneous and totalized TFF mass flow measurements during a simulated cascade fill are now considered. The mass flow uncertainty is based on the TFF mass flow equation

(Eq. 3) which has two terms: 1) the CFV mass flow and 2) storage effects in the connecting volume. Uncertainty components were assumed uncorrelated except where stated below and combined by root-sum-of-squares (RSS).

6.1 CFV mass flow uncertainty

Analysis of the basis equation for CFV mass flow (first term of Eq. 3) leads to the following expression for the uncertainty in the mass flow:

$$\frac{U(\dot{m}_{CFV})}{\dot{m}_{CFV}} = k \sqrt{\left(\frac{u_{C_d}}{C_d}\right)^2 + \left(\frac{u_{P_0}}{P_0}\right)^2 + \left(\frac{1}{2} \frac{u_{T_0}}{T_0}\right)^2}, \quad (4)$$

where U is the expanded uncertainty, $k = 2$ is the coverage factor for approximately 95 % confidence level, u is the standard 68 % confidence level ($k = 1$) uncertainty for the subscript quantities that have been previously defined. Eq. 4 uses normalized sensitivity coefficients which are unity for all but the stagnation temperature term, where the square root relationship between flow and temperature results in a normalized sensitivity coefficient of $\frac{1}{2}$. Components for the CFV throat area (A), the critical flow factor (C^*), and the universal gas constant (R) were omitted from Eq. 4 because they are correlated between calibration and usage of the CFV and are therefore negligible.

Working standard CFV mass flow uncertainty: 91 % of the operating flow range of the TFF CFV was calibrated by using working standard CFVs installed in series (as described in Section 2). The uncertainty of the working standard flows includes the uncertainty of: 1) the CFV calibrations against the $PVTt$ standard (0.013 %, $k = 1$), 2) pressure (0.02 %, $k = 1$), 3) temperature (0.03 %, $k = 1$), and 4) calibration stability over time (0.03 %, $k = 1$). These uncertainties summed in quadrature lead to a combined standard uncertainty for u_{C_d} of 0.05 % ($k = 1$). The pressure and temperature measurement uncertainties occur twice: first during calibration of the working standard CFVs and then again during their usage as references to calibrate the TFF CFV (the uncertainties are not correlated because different sensors were used on the two occasions).

TFF CFV discharge coefficient uncertainty: The C_d uncertainty includes components for the pressure (0.1 %, $k = 1$) and temperature (0.03 %, $k = 1$) measured during calibration against the working standards and the long term calibration stability of the discharge coefficient over the interval between periodic calibrations (0.03 %, $k = 1$). A significant uncertainty is introduced by changes in the gas species: the TFF CFV was calibrated using a nitrogen flow, but it is used to calibrate Coriolis meters in both nitrogen and helium. The species change introduces an estimated uncertainty of 0.02 % ($k = 1$) due to boundary layer thickness changes at the CFV throat [9]. The largest contributor is the pressure measurement for the TFF CFV.

Summarizing the prior paragraphs and returning to Eq. 4, u_{C_d}/C_d is 0.12 % ($k = 1$). The pressure and temperature uncertainty terms are highly dependent on the rate of change of the measurand and the time constant of the sensors used to measure them. At steady state conditions, the fast pressure and temperature sensors have uncertainties of 0.1 % and 0.03 %, respectively. But during the largest transients that occur upon opening the first HPT, the fast temperature and pressure sensors have uncertainties of 1.0 % and 12 %, respectively, ($k = 1$) Fig. 13. Taking the RSS of the uncertainty

components leads to an uncertainty for the mass flow from the CFV ranging from 12 % and 0.16 % ($k = 1$) depending on the stage of the HPT discharge.

The response time of a sensor determines both how fast the sensor will respond to a perturbation and how accurately it measures the magnitude of the perturbation. A first order instrument has a response equation [12]:

$$X_{\text{inf}} = \tau \frac{\partial y}{\partial t} + y ; \quad (5)$$

where τ is the sensor's time constant, $\partial y/\partial t$ is the rate of change of the measured parameter to a perturbation, y is the sensor's reading prior to the perturbation and X_{inf} is the predicted true value of the measured parameter. Eq. 5 can be used to deconvolute the temperature and pressure measurements to give a prediction of the actual temperature and pressure. The sensor's time constant is a function of the mass flow and hence Reynolds number. However, the time constants used in this work are treated as constants that are independent of the flow and determined at Reynolds values below that which the TFF operates. Therefore, the uncertainty in the difference between the predicted true temperature and pressure and the measured values is conservative. Experimental data for temperature and pressure at the CFV were used to generate smooth fits and $\partial y/\partial t$ was determined analytically for each profile. Figs. 13A and 13B show an example profile that includes the measured temperature and pressure, the predicted temperature and pressure if the sensors behave according to Eq. 5 and their associated uncertainties as a function of time. The percent difference between the deconvoluted and the measured values was taken as a $k = 1$ value and combined via RSS with the calibration uncertainties to obtain the uncertainty plotted as a function of time.

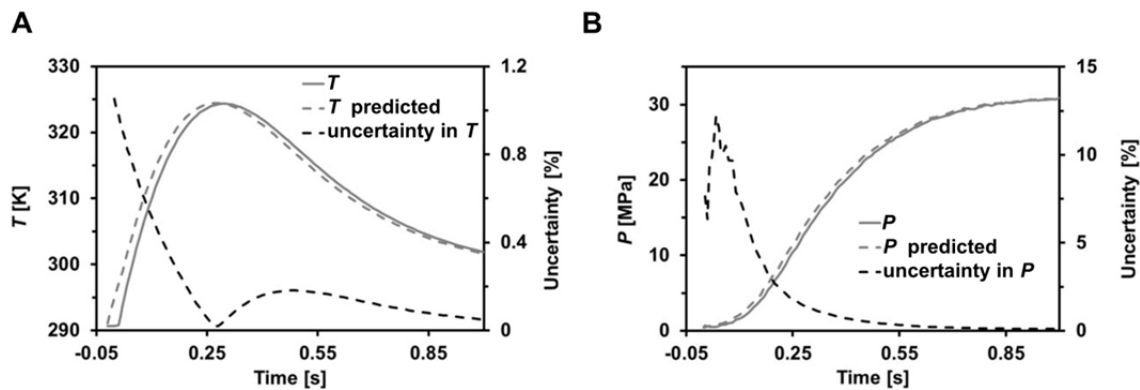


Figure 13. Example of the time-dependent uncertainty. A) The measured temperature, the predicted temperature and the uncertainty associated with the temperature measurement. B) The measured pressure, the predicted pressure and the uncertainty associated with the pressure measurement.

As predicted by Eq. 5, the uncertainty in the temperature and pressure measurements is greatest when the rate of change of these parameters is the largest. The temperature uncertainty has two

maxima that correspond to the periods of initial rise and subsequent fall. As the temperature and pressure rate of change diminishes, the uncertainty decreases to the steady state values.

6.2 Uncertainty due to storage effects in the connecting volume

Analysis of the second term of the TFF mass flow equation leads to the following uncertainty expression:

$$\frac{U(\dot{m}_c)}{\dot{m}_c} = k \sqrt{\left(\frac{u_{V_c}}{V_c}\right)^2 + \left(\frac{u_{\Delta\rho}}{\Delta\rho}\right)^2 + \left(\frac{u_{\Delta t}}{\Delta t}\right)^2}. \quad (6)$$

Eq. 6 uses unity normalized sensitivity coefficients. The connecting volume is 381 cm³ and has an expanded uncertainty of 0.6 % (determined by the volume expansion method [11]). Based on manufacturer's specifications and a comparison of the data acquisition computer clock against the NIST time standard, the time uncertainty is 0.05 % ($k = 1$). The uncertainty in the change in density is the largest contributor and ranges from 14 % during the largest transients that occur upon opening the first HPT to 0.4 % as the HPT depletes ($k = 1$).

The connecting volume had a single pressure sensor installed during the Coriolis meter measurements and hence a spatial average of pressure was unavailable. To assess the uncertainty involved with the lack of a spatial average, multiple pressure sensors were temporarily installed at strategic locations shown in Fig. 14A. These locations were based on the location of expected pressure drops due to valves and elbows and the heat exchanger. Fig. 14B shows the pressure profile in these sub volumes. It is apparent in Fig. 14B that the plumbing introduces significant pressure drops between the Coriolis meter outlet and the TFF CFV. The four pressure transducers have the same time constant and the visible lag of approximately 0.1 s is due to the time required for the flow to traverse the connecting volume.

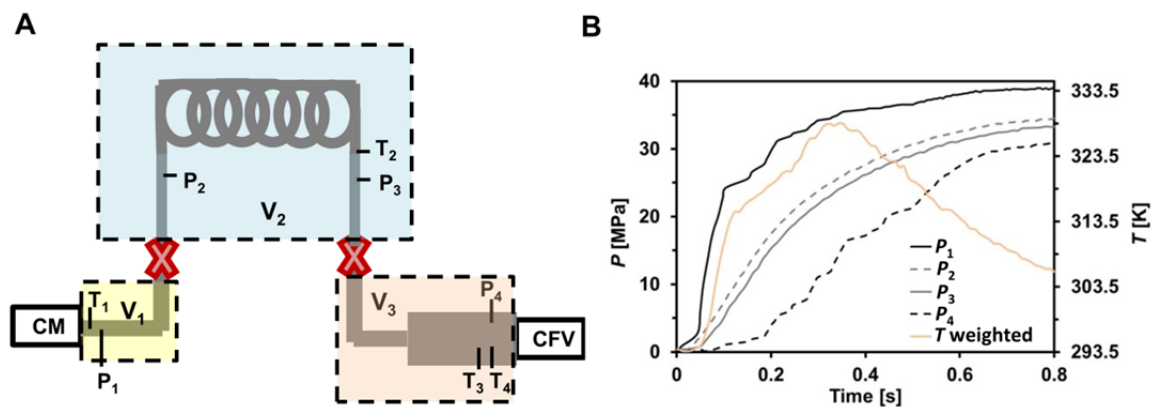


Figure 14. A) Schematic of the connecting volume and its sub-volumes, V_1 , V_2 and V_3 . V_2 contains the heat exchanger. B) Time traces of pressures in the connecting volume and the calculated volume weighted temperature.

An approximate spatial average pressure was calculated by weighting the four pressure measurements by the appropriate sub volume sizes:

$$P_W = \left(\frac{V_1}{V_{\text{total}}}\right)P_1 + \left(\frac{V_2}{V_{\text{total}}}\right)\frac{P_2+P_3}{2} + \left(\frac{V_3}{V_{\text{total}}}\right)P_4 = 0.02P_1 + 0.68\frac{P_2+P_3}{2} + 0.30P_4 \quad (7)$$

Based on the findings from the extra pressure sensors, a pressure correction factor = P_W/P_4 was applied to the single pressure measurement that was available for all Coriolis meter measurements. The pressure correction factor varies greatly as the connecting volume is filled (see Fig. 15) but it has been treated as a constant (1.08) for practical reasons. The practical difficulty is that during the discharge of four HPTs simulating a cascade fill, the pressure correction factor will not be consistent (*i.e.*, the value it peaks at and the time before it asymptotes to a constant is different for the discharge of each tank) and there is a time alignment problem between the Coriolis meter test data and the pressure correction measurement data.

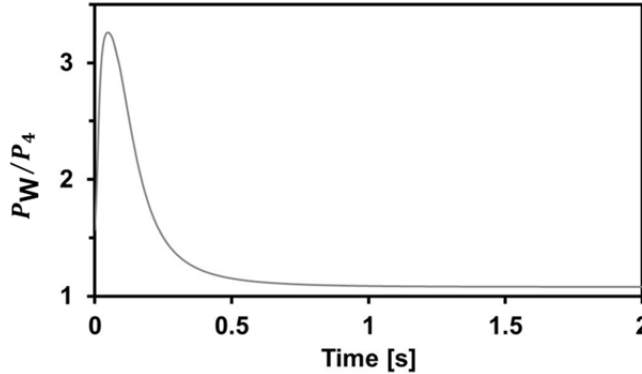


Figure 15. The pressure correction factor during the initial discharge of the first HPT when the pressure in the test section rises from approximately 0.7 MPa to 39 MPa.

The temperature spatial variation was not large; T_2 , T_3 and T_4 agreed within 0.1 % and T_1 only contributes 2 % to the volume weighted temperature. Therefore, only the weighted measurement is shown in Fig. 14B.

Because we are interested in how well we can measure the change in density, it is the rate of change in the temperature and pressure error that gives the uncertainty in the changing density. The

difference between the time varying correction factor and the constant value used (1.08) between adjacent time steps leads to the large uncertainty in the change in density in Eq. 6. Correlated uncertainties like calibration zero offsets cancel out and do not contribute to the uncertainty in the mass flow in the connecting volume. Therefore, it is the sensor response time and the use of a weighted pressure to correct data from the single sensor (P_4) that are the most significant components to the uncertainty in the density calculation.

The TFF will be instrumented with all four pressure sensors depicted in Fig. 14A in the future. This will reduce the uncertainty in the density to $< 1.6\%$ during the largest transients that occur in the facility and hence reduce the uncertainty in the instantaneous mass flow to $< 14\%$. Furthermore, the uncertainty of the facility to measure the totalized mass discharged by the four HPTs will be reduced by 0.05% .

6.3 TFF instantaneous mass flow uncertainty

The uncertainty in the instantaneous mass flow is given by:

$$\frac{U(\dot{m}_{\text{TFF}})}{\dot{m}_{\text{TFF}}} = k \sqrt{(S_{\dot{m}_{\text{CFV}}})^2 \left(\frac{u_{\dot{m}_{\text{CFV}}}}{\dot{m}_{\text{CFV}}}\right)^2 + (S_{\dot{m}_{\text{C}}})^2 \left(\frac{u_{\dot{m}_{\text{C}}}}{\dot{m}_{\text{C}}}\right)^2 + \sigma_{\text{noise}}^2} \quad (8)$$

In Eq. 8, the normalized sensitivity coefficients (S) are unity for the variance in the flow measurement, $\dot{m}_{\text{CFV}}/(\dot{m}_{\text{CFV}} + \dot{m}_{\text{C}})$ for the CFV mass flow, and $\dot{m}_{\text{C}}/(\dot{m}_{\text{CFV}} + \dot{m}_{\text{C}})$ for the connecting volume mass flow. From the mass flow normalized sensitivity coefficients it is clear that when the connecting volume flow is larger than the flow at the CFV, it contributes more to the uncertainty and vice versa.

The variance of the flow measurement, σ_{noise}^2 , which is the standard deviation of five consecutive flow measurements is a large contributor (up to 99.7%) to the instantaneous flow measurement uncertainty. The other significant contributor is $\Delta\rho$, which is traceable to the response times of the temperature and pressure sensors. Fig. 16 shows the mass flow with the associated uncertainty limits ($k = 2$). The expanded uncertainty in the instantaneous mass flow is as high as 24% at the initial discharge of a HPT (because of the uncertainty associated with \dot{m}_{C}), and it decreases to 14% as the tank depletes.

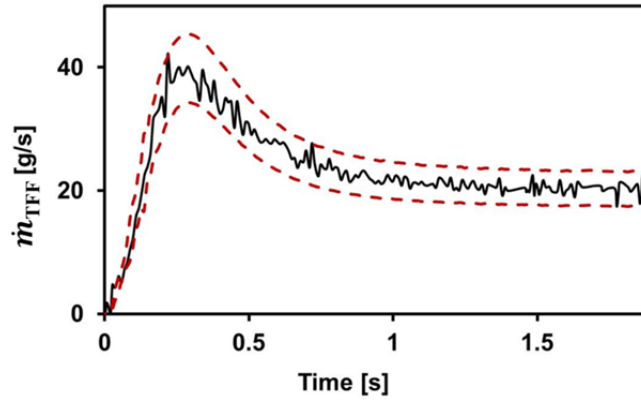


Figure 16. The mass flow of helium as one HPT discharges and the uncertainty bounds for the instantaneous mass flow ($k = 2$).

6.4 Totalized mass flow uncertainty

The uncertainty in the totalized mass flow is given by Eq. 8, however, the variance of the flow measurement (σ_{noise}^2) is negligible for the totalized mass metered because the noise is centered on the mean value and cancels out when the integral of the mass flow is calculated. Therefore, the largest contributing components to the uncertainty in totalized mass metered are C_d and \dot{m}_c . The two main uncertainty components in Eq. 8 can be further divided into the sub components listed in Table 3. Table 3 lists all of the considered mass flow uncertainty components, including uncertainties from calibration and from possible impurities in the helium gas that affect the molecular weight (M) and C^* .

Table 3. Normalized sensitivity coefficients S , relative uncertainties u_c , and the relative contributions of the uncertainty components for the totalized mass metered. Both minimum and maximum values are given as the component value greatly depends on the instantaneous flow.

<u>Total Mass Metered</u>				
Uncertainty component	Nominal Value	S min to max	u_c ($k = 1$, %) min to max	% contribution min to max
C_d	0.96	0.12 to 1.8	0.12	.01 to 99.98
P_0	15 to 30 [MPa]	$< 1 \times 10^{-6}$	0.1 to 12	< 0.01
T_0	290 to 329 [K]	$< 1 \times 10^{-6}$	0.03 to 1.0	< 0.01
V_{Inv}	381 [cm ³]	-0.01 to 0.84	0.6	< 0.01 to 6.8
$\Delta\rho$	0 to 0.001 [kg/m ³]	-0.01 to 0.84	0.4 to 14	< 0.01 to 18.0
A	0.8 [mm ²]	$< 1 \times 10^{-6}$	< 0.01	< 0.01
C^*	0.7	$< 1 \times 10^{-6}$	< 0.01	< 0.01
M	.004 [kg/mol]	$< 1 \times 10^{-6}$	< 0.01	< 0.01

R	8.314 [J/(mol K)]	$< 1 \times 10^{-6}$	< 0.01	< 0.01
----------	-------------------	----------------------	----------	----------

To determine the uncertainty in the totalized mass metered, the area under the mass flow curve was compared to that of the mass flow curve with the upper and lower uncertainty bounds included. The TFF is capable of measuring the totalized mass discharged from the HPTs in a cascade type refilling scenario to within 0.45 % ($k = 2$).

7. Summary and Conclusions

7.1 Capabilities of the Transient Flow Facility

NIST's Transient Flow Facility (TFF) is a closed loop that consists of four pressurized tanks (42 MPa) that discharge sequentially through the meter under test to mimic cascade gaseous refueling. The pressure at the meter under test reaches 39 MPa.

The TFF's expanded uncertainty ($k = 2$) in instantaneous mass flow ranges from 14 % to 24 % depending on the flow. This uncertainty is driven by variance of the flow measurement and the changing density in the volume connecting the Coriolis meter and the CFV. It is critical to account for storage effects in the connecting volume because 0.5 s after the initial discharge of one pressurized tank the flow in this volume is as much as 7 times that through the TFF CFV. The TFF's expanded uncertainty for the totalized mass metered is 0.45 % ($k = 2$). The variance of the flow measurement is negligible for the totalized mass metered because the noise is centered on the mean value and cancels out when the integral of the mass flow is calculated. Therefore, the largest contributing components to the uncertainty in totalized mass metered are the CFV discharge coefficient and the changing density in the connecting volume.

In this work, the TFF was used to measure the performance of two Coriolis meters for a particular transient protocol. However, the TFF is capable of testing other meter types and protocols, thus making it ideal for testing prototype field calibration standards for gaseous fuel dispensers. More generally, the TFF is capable of a wide variety of tests dealing with transient pressure, temperature, and flow conditions, including gaseous refueling processes, blow-downs, and quasi-stable calibrations.

7.2 Performance of Coriolis meters A and B

Three Coriolis meter calibration options were tested: 1) "As received calibration and field zeroing": the as received calibration was used with a field zeroing with the Coriolis meter's user interface; 2) "additional zeroing": the Coriolis meters indicated a negative flow under the no flow condition despite the field zeroing procedure, and this negative zero flow reading was subtracted from the acquired flow data before integration; and 3) "additional zeroing and calibration": the negative zero flow reading was removed as for option 2 and a gain correction was applied based on the TFF steady state flow calibration shown in Figs. 6A and 6B.

Both meters were tested in nitrogen and helium and with different meter settings (*i.e.* lag, time constant, low flow cut-off limit, and low pass filter where applicable). The meter settings that allow for the fastest response should be used for transient flow measurement. In comparison with the nitrogen tests, our helium tests more closely approximate the behavior expected during hydrogen re-fueling; therefore, the values in the last row of Table 1 and of Table 2 are the most important test results. Both Coriolis meters were found to be capable of measuring transient flows within the desired

maximum permissible errors for meters used in gaseous refueling dispensers [1.0 %, OIML R 139 2007] regardless of which calibration option was employed. Coriolis meter A agreed with the TFF within its uncertainty when calibration options 2 or 3 were used. Coriolis meter B agreed with the TFF within its uncertainty regardless of which calibration option was used.

8. Acknowledgements

The authors would like to thank Dr. John Hurly for his aid in the design and procurement of parts for the Transient Flow Facility.

9. References

-
- [1] OIML R 139 Edition 2007(E), International Recommendation: Compressed gaseous fuel measuring systems for vehicles, International Organization of Legal Metrology, section 3.1.1, page 14.
- [2] Cascetta, F., Rotondo, G., and Musto, M. Measuring of compressed natural gas in automotive application: A comparative analysis of mass versus volumetric metering methods. *Flow Meas. Instrum.* 2008; 19: 338 – 41.
- [3] Wright, J. D, and Johnson, A. N. Uncertainty in primary gas flow standards due to flow work phenomena. *Proceedings of the International Flow Measurement Conference: FLOMEKO 2000*; Salvador, Brazil.
- [4] Wright, J. D. and Johnson, A. N. NIST lowers gas flow uncertainties to 0.025 % or less. *NCSL International Measure* 2010; 5: 30 – 39.
- [5] Wright, J. D., Performance of critical flow venturis under transient conditions. *Meas. Sci. Technol.* 2010; 21: 055404 doi:10.1088/0957-0233/21/5/055404.
- [6] Johnson, A. N., Espina, P. I., Wright, J. D., Mattingly, G. E., Merkle, C. L. Numerical characterization of the discharge coefficient in critical nozzles. *Proceedings of the NCSL Workshop and Symposium 1998*; Albuquerque, NM.
- [7] Lemmon, E. W., Huber, M. L., and McLinden, M. O. Refprop 23: Reference fluid thermodynamic and transport properties. *NIST Standard Reference Database 23*, Version 9 2010; National Institute of Standards and Technology, Boulder, CO.
- [8] A. N. Johnson. Numerical characterization of the discharge coefficient in critical nozzles. Ph.D. Dissertation. 2000; Pennsylvania State University, College Station, PA.
- [9] Johnson, A. N. Natural gas flow calibration service. Special Publication: NIST SP250-1081, 2008.
- [10] Wright, J. D. What is the “best” transfer standard for gas flow?. *Proceedings of the International Flow Measurement Conference: FLOMEKO 2003*; Groningen, Netherlands.

[11] Wright, J. D., Johnson, A. N., and Moldover, M. R. Design and uncertainty analysis for a *PVTt* gas flow standard. *J. Res. Natl. Inst. Stand. Technol.* 2003; 108: 21 – 47.

[12] Coleman, H. W., Steele, W. G. Experimentation, validation, and uncertainty analysis for engineers. 3rd ed. New Jersey: John Wiley & Sons Inc.; 2009.